International Communications in Heat and Mass Transfer 126 (2021) 105418

Contents lists available at ScienceDirect

International Communications in Heat and Mass Transfer

journal homepage: www.elsevier.com/locate/ichmt

Extensive examination of sonication duration impact on stability of Al_2O_3-Polyol ester nanolubricant

A. Nugroho [a,b,*], Z. Bo [a], R. Mamat [a,b], W.H. Azmi [b], G. Najafi [c], F. Khoirunnisa [d]

[a] School of Mechanical Engineering, Ningxia University, China
[b] College of Engineering, Universiti Malaysia Pahang, Pekan, Pahang, Malaysia
[c] Department of Biosystems Engineering, Tarbiat Modares University, Tehran, Iran
[d] Department of Chemistry, Indonesia University of Education, Bandung, Indonesia

ARTICLE INFO

Keywords:
Absorbance
Al_2O_3 nanoparticles
Al_2O_3-POE nanolubricants
UV visible
Sonication

ABSTRACT

The sonication technique is one of the effective methods to stabilize nanolubricants. This paper aims to elaborate on the sonication duration's impact on the stability of Al_2O_3-Polyol ester nanolubricants. A two-step method has been performed to prepare nanolubricants. Each sample consisted of a nanoparticle mixed with POE using a magnetic stirrer without surfactant for 30 min. All samples had the same volume concentration, namely 0.02 vol % but received different interlude sonication duration treatments for 0, 40, 60, 80, 100, and 120 min. FESEM with Energy Dispersive X-Ray was used to characterize the Al_2O_3 nanoparticle sample's morphology and element analysis. UV Visible and absolute zeta potential were used to determine Al_2O_3-POE nanolubricants stability. The findings show that the most optimal sonication impact in this study is 80-min sonication. It proofed by the highest absorbance ratio among other samples, which is 0.411, the lowest drop absorbance value, which is 58.9%, and and with a zeta potential value of 45 mV. The rheological behavior analysis shows that Al_2O_3-POE nanolubricants show Newtonian behavior.

1. Introduction

It has been well recognized that both mineral and synthetic oil are widely used as lubricants in engineering applications [1–4]. Lubricants' purpose includes reducing friction, wear, the heat between mechanical parts and improving cooling productivity [5]. Conventional coolants like water, ethylene glycol, propylene glycol, and oils possess low thermal conductivity, which hinders improving system thermal efficiency [6,7]. Modern engineering applications are currently requiring an advanced lubricant to improve their machinery productivity and prevent them from the mechanical trip of overheating due to its workloads [8–12]. This issue can be solved by dispersing nanoparticles into the conventional fluid as the base fluid [13–16]. Active and passive cooling methods are the two possible methods for removing heat. An advanced class fluid known as "Nanofluids" was initially introduced by Masuda et al. [17] and Choi [18]. Matsuda et al. dispersed ultra-fine powders of Al_2O_3, SiO_2, and TiO_2 in water as the liquid. Choi reported that an innovative new class of heat transfer fluids could be engineered by suspending metallic nanoparticles in conventional heat transfer fluids. Nanofluids consisting of such particles suspended in liquids (typically conventional heat transfer liquids) enhanced the thermal conductivity [19] and convective heat transfer performance of the base liquids [20]. The resulting "nanofluids" are expected to exhibit high thermal conductivities compared to those currently used heat transfer fluids [21]. Previous researchers around the globe have done several studies regarding sonication impact on nanoparticle dispersion [20–24] and thermal conductivity of nanofluids improvement [25–30] to improve the heat transfer rate of nanofluids [34,35]. This paper will elaborate on the effect of interlude sonication treatment on the stability of Al2O3-POE lubricant without additional surfactant based on the absorbance value of UV visible assessment.

Magnetic stirring and sonication duration are two significant factors that affect nanofluids stability. Karthikeyan et al. [36] suspended CuO nanoparticles by homogenizing them using an ultrasonic horn (Vibronic ultrasonic processor P1–250 W) for 30 min without surfactants. Caixiang et al. [37] reported the stability of CeO_2 and $CaCO_3$ nanolubricants was developed by employing a magnetic force mixer for two h at 80 °C. Liu et al. [38] demonstrated an enhancement of thermal conductivity with carbon nanotube for nanofluids. The mixture was blended by a magnetic stirrer and mixed up by an ultrasonic homogenizer. Carbon nanotube–synthetic engine oil suspension, thermal conductivity was

* Corresponding author at: School of Mechanical Engineering, Ningxia University, China.
E-mail addresses: ir.agusnug@gmail.com (A. Nugroho), 12712580@qq.com (Z. Bo), rizalman@ump.edu.my (R. Mamat).

https://doi.org/10.1016/j.icheatmasstransfer.2021.105418

Nomenclature

min	Minute
h	Hour
vol%	Volume %
POE	Polyol ester
UV Vis	Ultra Violet visible
T	Temperature (°C)
FESEM	Field-Emission Scanning Electron Microscopy
TEM	Transmission Electron Microscopy
Greek symbols	
ϕ	Volume concentration (%)
ρ	Density (g/cm^3)
Subscripts	
L	Lubricant
P	Nanoparticle
nf	Nanofluid
bf	Base fluid

Table 1
Al_2O_3 physical nanoparticles properties.

Properties	Metric
Density	3.95 g/cm^3
Molar mass	101.96 g/mol
Diameter	13 nm
Color	White
Melting point	2040 °C
Boiling Point	2977 °C

Table 2
Properties of Polyol ester oil.

Oil	Properties					
	Viscosity at 40 °C	Viscosity at 100 °C	Viscosity Index	Density at 15 °C	Flash Point	Pour Point
Suniso SL 68	70.1 cSt	9.1 cSt	105	0.960 g/cm^3	252° C	−36 °C

enhanced by 30% at a volume fraction of 0.02 vol%. Later, Pang et al. [39] reported that the thermal conductivity of Al_2O_3 and SiO_2 methanol-based nanofluids increased with an increase of the nanoparticle volume fraction, and the enhancement was observed to be 10.74% and 14.29% over the base fluid for the concentration of 0.5 vol% of Al_2O_3 and SiO_2 nanoparticles, respectively. The suspension was dispersed by using the ultrasonic vibration for 2 h to break down the agglomerations and improve the stability. Ruan et al. [40] observed that the sonication process reduced the sizes and length of carbon nanotubes. Asadi et al. [41] reported that 30 min was the optimum sonication time for stability. Beyond that sonication duration, it leads to the destruction of nanofluids' stability and thermal properties.

In the present study, the interlude sonication impact on Al_2O_3-POE nanolubricants samples has been investigated. Most of the recent studies reported that there might be an optimum duration for better dispersion stability. However, this may not necessarily be the most prolonged ultrasonication duration tested. Therefore, this paper aims to elaborate on the extensive examination of sonication impact treatment using the interlude sonication method on newly prepared Al_2O_3-POE nanolubricants systematically by discussing the nanolubricants' absorbance values extensively and their ratio study. The experimental assessment utilizing UV visible spectrophotometer to determine the most optimum sonication treatment duration. The measurements were taken after sample preparation and after 15 days to all samples.

2. Experimental procedure

2.1. Materials

Aluminum oxide nanoparticles, 99.99% trace metals basis nanoparticles, were purchased from Sigma-Aldrich, Saint Louis, the USA, for this study. Table 1 shows the Al_2O_3 specification and Al_2O_3 nanoparticles' thermal properties. The polyol ester (POE) lubricant, a synthetic refrigerant oil, was purchased from SUNISO from Belgium. POE lubricant's essential properties are listed in Table 2. The two-step method was employed to prepare nanolubricants as suggested by Ali et al. [42], Mohammed et al. [43], and Nabil et al. [44] with a volume fraction of 0.02% nanoparticles in all samples with the same mixing duration but different ultrasonication ranging from 30 to 120 min with an interlude of 15 min every 40 min cycle.

Al_2O_3 is an essential element of ceramic oxides that has been used by previous researchers in their study [45–48]. Alumina is used in the chemical industry, metallurgy, and other industrial applications due to its performance, morphology, and thermal properties. The surface of mostly ceramic nanoparticles such as alumina is polar and hydrophilic since they do not disperse in organic environments [49].

2.2. Nanolubricants preparation method

The magnetic stirrer device operated without a heater at the rate of 600 rpm. The ultra-sonication device Fisherbrand™ from FisherScientific operated at 37 kHz. Fig. 1 shows how Al_2O_3 nanoparticles are mixed with POE lubricant in the magnetic stirrer and ultrasonication treatment. They are treated in an ultrasonication bath for the agglomeration breakdown process, respectively.

Three stages were required to prepare the nanolubricants. The initial stage involved Al_2O_3 nanoparticles and POE lubricant measurement. The nanoparticles were measured using the digital weighing scale Sartorius Entris to determine the required mass of Al_2O_3 nanoparticles and POE lubricant before the mixing process. Previously, the balance was calibrated to reach a reasonable level and adjust the circle centre's levelling bubble. The medial stage involved mixing the base lubricant (POE lubricant) and Al_2O_3 nanoparticles utilizing a magnetic stirrer for 30 min. The third stage involved the ultrasonication process utilizing an ultrasonic bath to breakdown the nanolubricants agglomerations between 30, 40, 60, 80, 100, and 120 min. Eq. (1) is used to calculate the volume fraction of the nanolubricants as suggested by Mahbubul et al. [50], Das et al. [51], Nabil et al. [44], and Elsaid et al. [52]. After each 40-min cycle, a 15-min interlude was applied to prevent nanolubricants' homogeneity damage.

$$\varnothing = \frac{m_p/\rho_p}{m_p/\rho_p + m_l/\rho_l}\ x\ 100\% \tag{1}$$

Where φ is the nanoparticle concentration in volume %; m_p and m_l are the masses of the nanoparticle and lubricant, respectively; and ρ_n and ρ_r are the density of the Al_2O_3 nanoparticle and POE lubricant, respectively.

3. Results and discussion

3.1. Al2O3 nanoparticles characterization

Zawawi et al. [53] and Sadoun et al. [54] employed Field-Emission Scanning Electron Microscopy (FESEM) to characterize the morphology of Al_2O_3 and other nanoparticles. To confirm Al_2O_3 nanoparticles' morphology and shape, in this study, Field-Emission Scanning Electron Microscopy (FESEM) JSM-7800F from JEOL Ltd. was employed

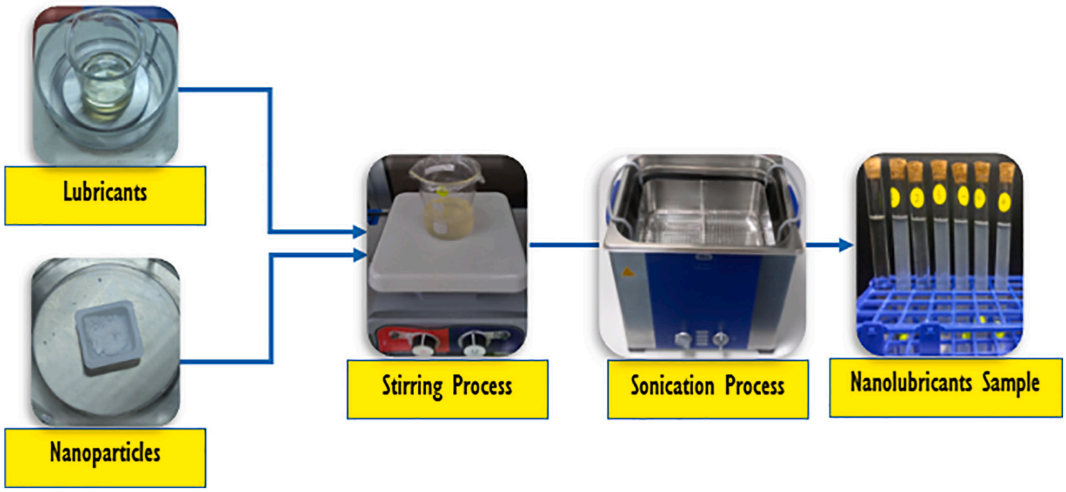

Fig. 1. Al_2O_3-POE nanolubricants preparation using the two-step method.

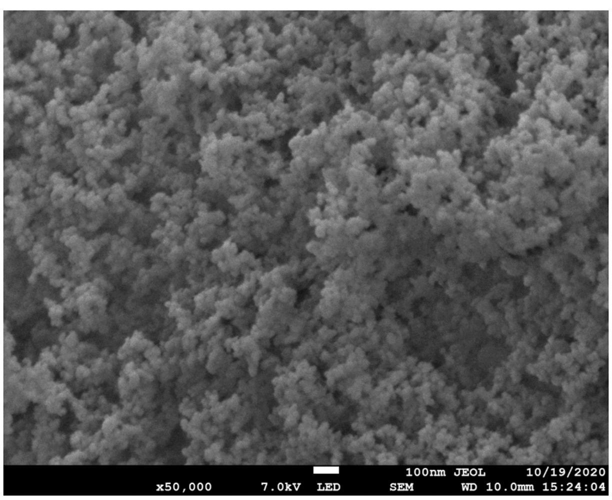

Fig. 2. Al_2O_3 Nanoparticles morphology in 50,000 magnification.

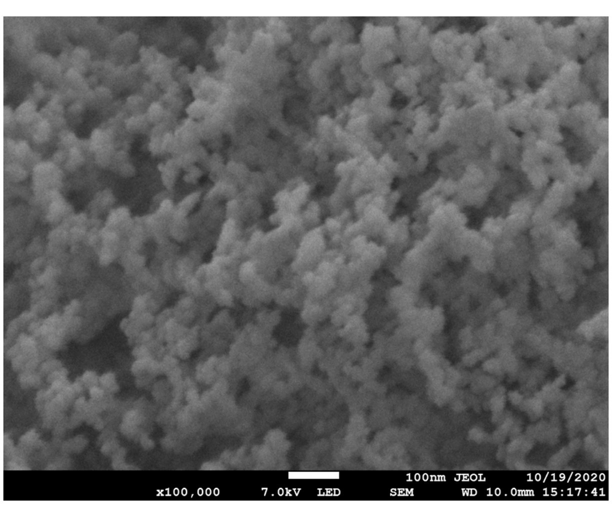

Fig. 3. Al_2O_3 Nanoparticles morphology in 100,000 magnification.

to characterize the morphology, size, and shape of the Al_2O_3 nanoparticles.

The graph was captured using an LED menu of 7.0 kV with a magnification scale of 50,000× and 100,000×, respectively, as shown in Figs. 2 and 3. The data consist of Al_2O_3 nanoparticles microstructure at the molecular level. Instead of macrostructure [55], similarly previous researchers employed FESEM to determine the nanoparticles morphology and its microstructure [56–58].

Based on the results of the FESEM characterization in Fig. 2, it can be seen that the morphology of dry Al_2O_3 has a uniform shape, which is round and has a uniformity level of size with an average grain size of 13.3 nm shown in Fig. 3.

3.2. Al_2O_3 nanoparticles element analysis

In order to confirm the formation of Al_2O_3 nanomaterials, Energy Dispersive X-Ray (EDX) analysis was performed as suggested by Wagih et al. [59], Sofiah et al. [60], Sahoo et al. [61], Pourrajab et al. [62] and other previous researchers [63–65]. During the EDX measurement, different areas were focused, and the corresponding peaks are shown in Fig. 4.

The spectrum shows only major elements Al and O showing, meaning it shows the purity of the nanoparticles. The analysis consists of spectra showing peaks corresponding to the elements making up the actual composition of the sample of Al_2O_3 nanoparticles analyzed, as shown in Fig. 4. According to the EDX spectra result, the larger the peak, the larger the element, representing the particular material element. Similarly, previous researchers [66–68] employed EDX analysis to determine the Al_2O_3 nanoparticles elemental analysis. Sadoun et al. [69] explained that examining element microstructure and morphology of nanoparticles with an XRD-connected FESEM is very accurate.

Table 3. provides the percentage of elements in Al_2O_3 nanoparticles by EDX analysis. Two dominant elements were found in the sample. The elements were oxygen (O) and Aluminum (Al), with a weight percentage of 61.53% and 38.47%. Al_2O_3 was a chemical compound in oxide form, and oxygen element dominated it. Thus, the oxygen percentage of the element was higher than another element [70]. Elements that are not linked to the constituent elements of Al_2O_3 have been overlooked to remove uncertainty in the EDX review. The peak of the highest peak shown in Fig. 4, a carbon element derived from the EDX-detected carbon type.

Because Al_2O_3 was non-conductive material in nature, the surface of the Al_2O_3 nanoparticle acted as an electron trap. Therefore, a sputter coating had been done before the characterization. Otherwise, the increase of electrons (charged) on the nanoparticle's surface would generate extra-white regions on the sample. This extra-white region influenced the image information during the characterization process. Once sputter coating was utilized, the conductive coating created a

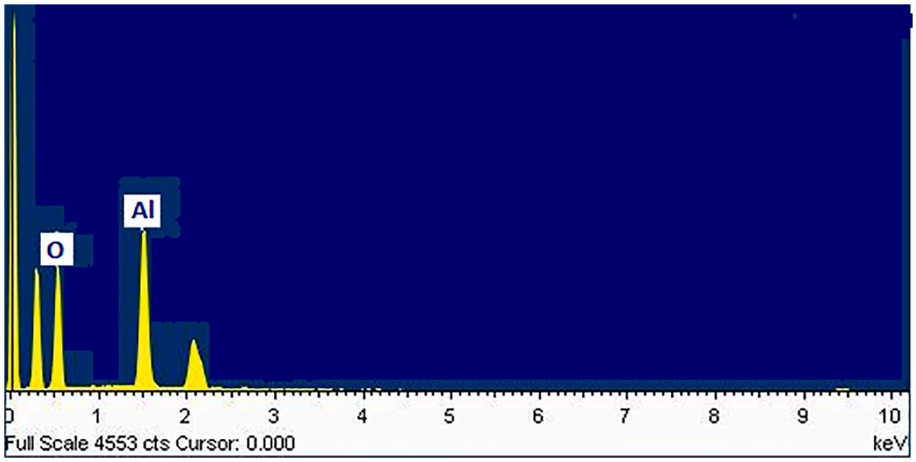

Fig. 4. EDX element analysis of Al_2O_3 Nanoparticle.

Table 3
Element percentage of Al_2O_3 by EDX.

Element	Weight %	Atomic %
Oxygen	61.53	72.95
Aluminum	38.47	27.05
Total	100.00	–

channel that allowed the charging electrons to be detached from the nanoparticle surface.

Platinum sputter coating was used in this study. There are some advantages of using Platinum; (i) it has a finer grain size than gold or gold-palladium, (ii) it is more suitable for higher magnifications applications, (iii) it is resistant to "stress cracking" when oxygen is present (a porous sample may be a source of oxygen). Dry samples of Al_2O_3 nanoparticles had been mounted on the carbon type. The sample positioning was done very carefully and did not press the sample's surface to avoid changes in the surface morphology of the sample particles.

The coating thickness was between 2 and 3 nm due to the optimum thickness; otherwise, the platinum element would dominate the primary element of Al_2O_3 nanoparticles if it was beyond 3 nm or would be less conductive if it was less than 2 nm.

3.3. Visual stability analysis

Nanolubricants sample comparison is shown in Fig. 5. It is to observe the level of nanolubricants stability as done by previous researchers [71–74]. Observations were made to observe whether agglomeration and sedimentation occurred and determined the sample stability visually. Fig. 5 (a) shows the Al_2O_3/POE nanolubricants samples just after the preparation.

From the samples, it can be seen that Al_2O_3 nanoparticles are very well dispersed with POE lubricants. Sample 0 was a POE lubricant without any nanoparticles addition, and sample 1 was Al_2O_3/POE nanolubricants that stirred for 30 min without sonication treatment. Meanwhile, samples 2, 3, 4, 5, and 6 were Al_2O_3-POE nanolubricants samples that experienced 30 min stirring and ultrasonic treatment for 40, 60, 80, 100, and 120 min respectively. The interlude sonication treatment process is shown in Fig. 6.

Fig. 5(b) shows the display of the Al_2O_3/POE nanolubricants sample on day 15th. There are different visualizations on day 15th. Sedimentation and agglomeration in sample 1 were significant, as nanoparticles were deposited at the experimental channel's bottom. Different conditions were also in samples 2, 5, and 6. This agglomeration phenomenon in nanolubricants was due to Van deer Walls' force between

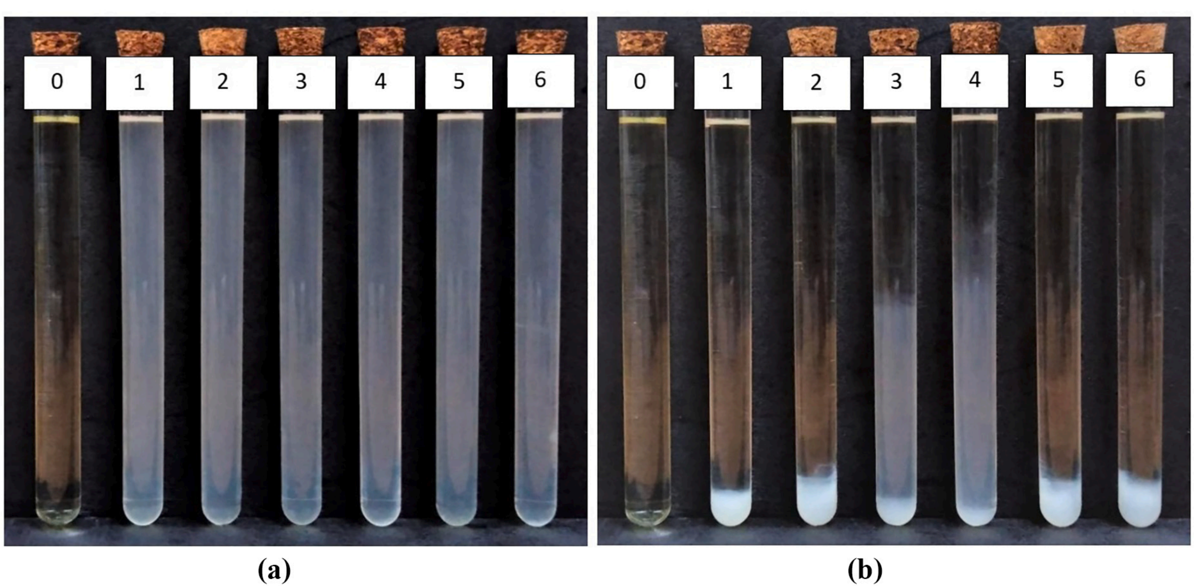

Fig. 5. Al_2O_3/POE nanolubricants sample in (a) day 1 and (b) day 15.

Fig. 6. Ultrasonication treatment process on Al_2O_3/POE nanolubricants.

nanoparticles at the atomic level [75,76]. Samples 3 and 4 looked better than the rest of the samples. Agglomeration and sedimentation occurred throughout samples 3 and 4 but did not drop to the maximum level at the experimental tube's bottom. It concludes that a good sonication treatment duration under these conditions is between 80 and 100 min.

Nevertheless, it cannot be said that these two samples are stable even though they visually show better conditions than samples 1, 2, 5, and 6. Previous researchers had consistently proposed obtaining stable nanolubricants before apparatus implementation [77,78]. Visual observation for 15 days and UV visual examination was performed in this study to establish the stability of the Al_2O_3-POE nanolubricants as the previous researchers [79,80] did. In this analysis, unlike previous researchers, nanoparticles were well dispersed on a specially formulated synthetic lubricant for electric motors application. Nanolubricants stability could be predicted by analyzing the result of UV visible analysis. These two approaches are commonly used in literature by various researchers [81,82].

3.4. Absorbance studies analysis

Understanding the definition of absorbance and transmittance is crucial before the experiment. Absorbance is the quantity of light absorbed by a nanolubricant, whereas transmittance is the quantity of light that passes through nanolubricants. The schematic of absorbance studies utilizing UV visible is shown in Fig. 9.

Absorbance analysis utilizing a UV visible spectrophotometer approach is one of the most potent methods to assess the stability of nanolubricants by the absorption of transmitted light passing nanolubricants [83].

The visible UV provides the desired spectrum of light wavelength. Second, the lens transmits a straight beam of light (photons) that passes through a monochrome to separate it into many wavelength components (spectrum). The wavelength selector then transmits only the desired wavelengths, as shown in Fig. 7. After the target spectrum of light wavelength passes through the nanolubricants in the cuvette, the photometer measures the photons' sum. The photons are absorbed, and then they send a signal to the galvanometer or digital display.

The absorbency is proportional to the percentage of the particles contained in the nanolubricants. The nanolubricants sample is exposed to incident light. The higher absorbance value indicates the higher concentration of nanoparticles in a particular scanned area. UV visible assessment has been performed for all nanolubricants samples and the findings are shown in Fig. 9. UV visible assessment of Al_2O_3-POE nanolubricants was conducted using Thermo Scientific™ GENESYS™ 50 UV Visible spectrophotometer as shown in Fig. 8. It is a single-cell configuration UV visible measurement that assesses sample absorbance value up to 5 points of absorbance unit.

UV visible assessment was performed using scan mode, and here the wavelength was scanned while the ordinate value was recorded to generate a spectrum. The spectrophotometer scanned from the longest wavelength (1100 nm) to the shortest wavelength (200 nm). This was to reduce the sample's cause of photo-decomposition. The assessment was conducted on the first day immediately after the preparation of nanolubricants as suggested by Mamat et al., [84] and Gallego et al. [85].

It was observed that the absorbance in nanolubricants first increased and then decreased after reaching a peak at a particular wavelength, as shown in Fig. 9. Fig. 9 shows the experimental result of Al_2O_3-POE nanolubricants based on screen-printed Al_2O_3 of every sample. It indicates a broad absorption spectrum in the UV–Visible region and shows significant absorbance as reported Kawai et al. [86] and Xian et al. [87]. The display can see the effects of the calculation of the absorbance of Al_2O_3-POE nanolubricants. The graph shows that all of the sample charts travel from the longest wavelength of 1100 nm to the shortest wavelength of 200 nm. In general, there is no substantial increase in all wavelength samples from 1200 to 370 because the samples have the same concentration, which is 0.02 vol%. However, both samples undergo their respective absorption peaks at wavelengths 360, 302, 278, and 218 nm are 2, 1, 4, and 2 points, respectively. It can, therefore, be argued that the Al_2O_3-POE nanolubricants exhibits significant absorbance. Fig. 10 demonstrates the correlation between the wavelength

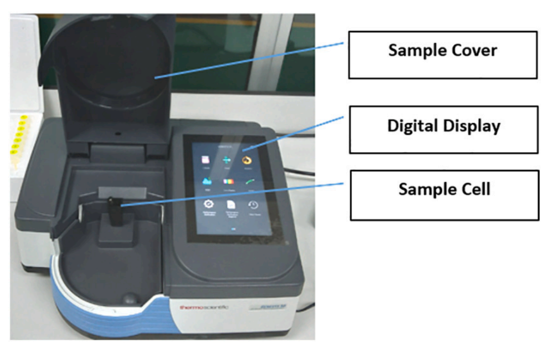

Fig. 8. Thermo Scientific™ GENESYS™ 50 UV Visible spectrophotometer.

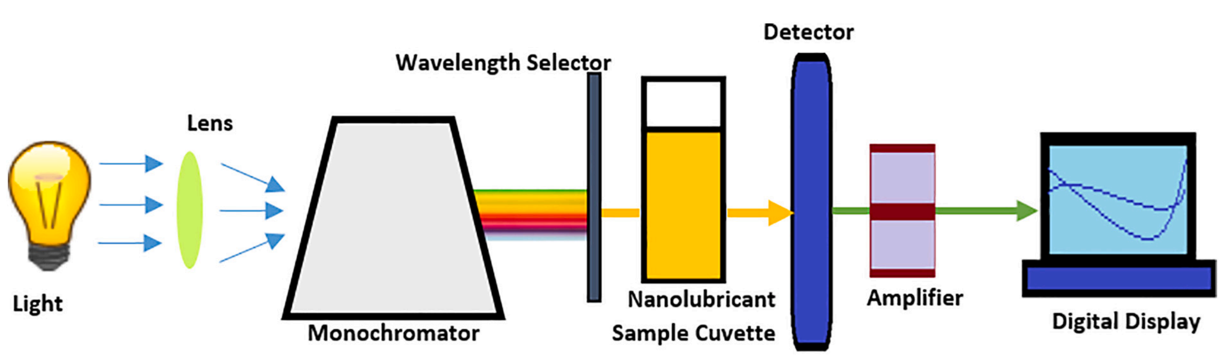

Fig. 7. Schematic diagram of absorbance process in UV Vis Spectrophotometer.

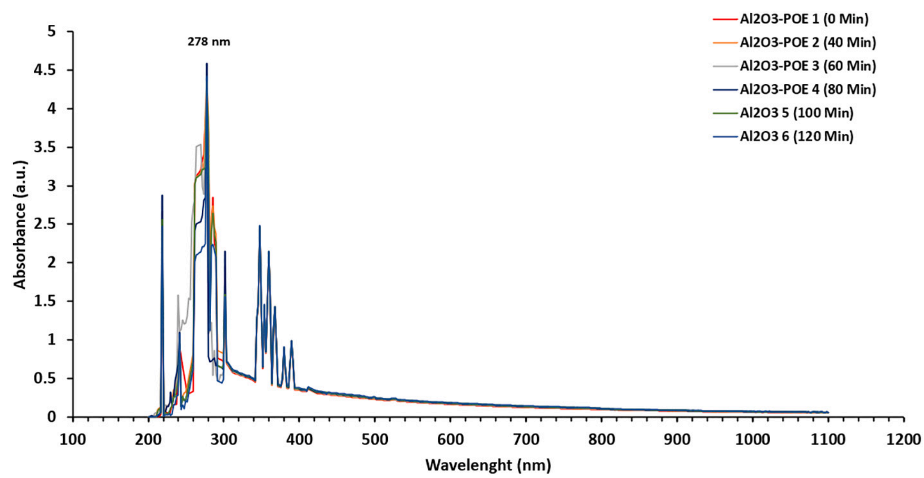

Fig. 9. Absorbance distribution of Al2O3-POE in every test on day 1.

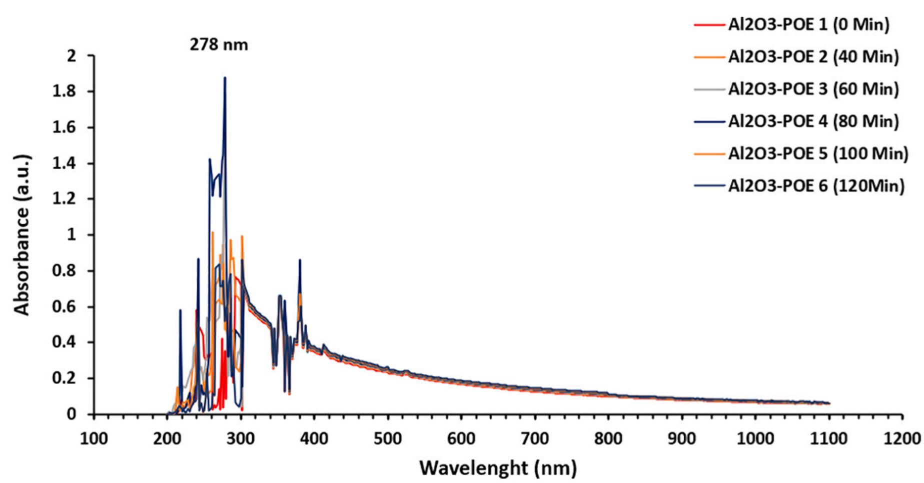

Fig. 10. Absorbance distribution of Al2O3-POE in every test on day 15.

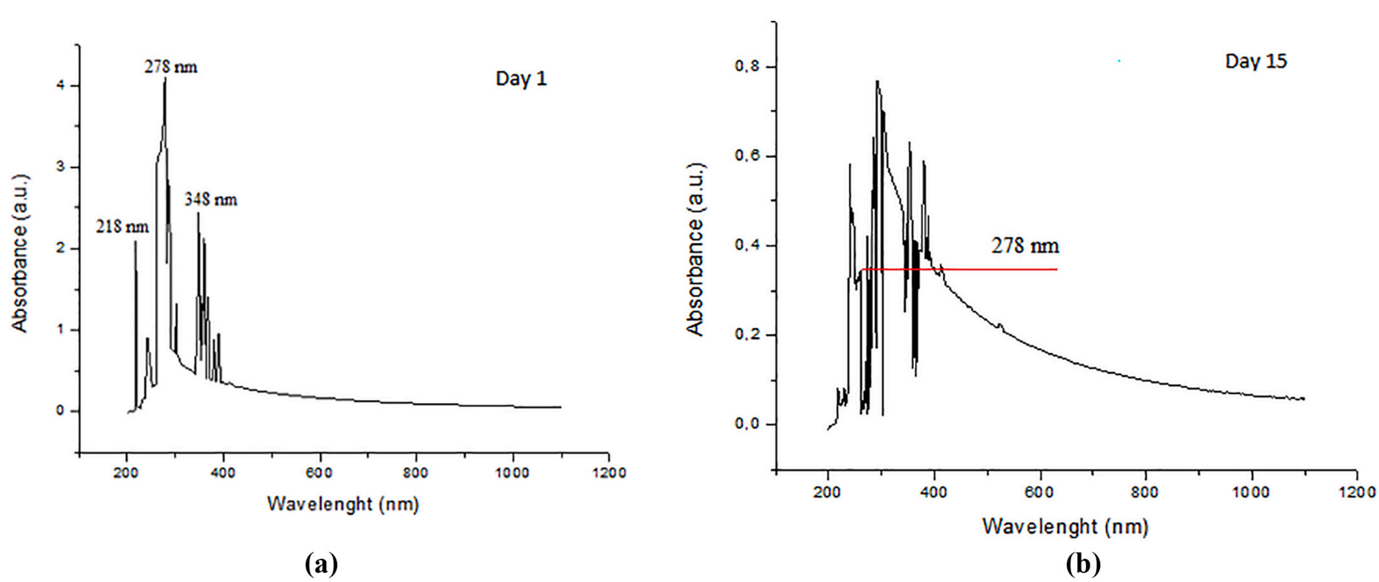

Fig. 11. The absorbance value of Al_2O_3-POE nanolubricants with 0 min sonication (a) day 1 (b) and day 15.

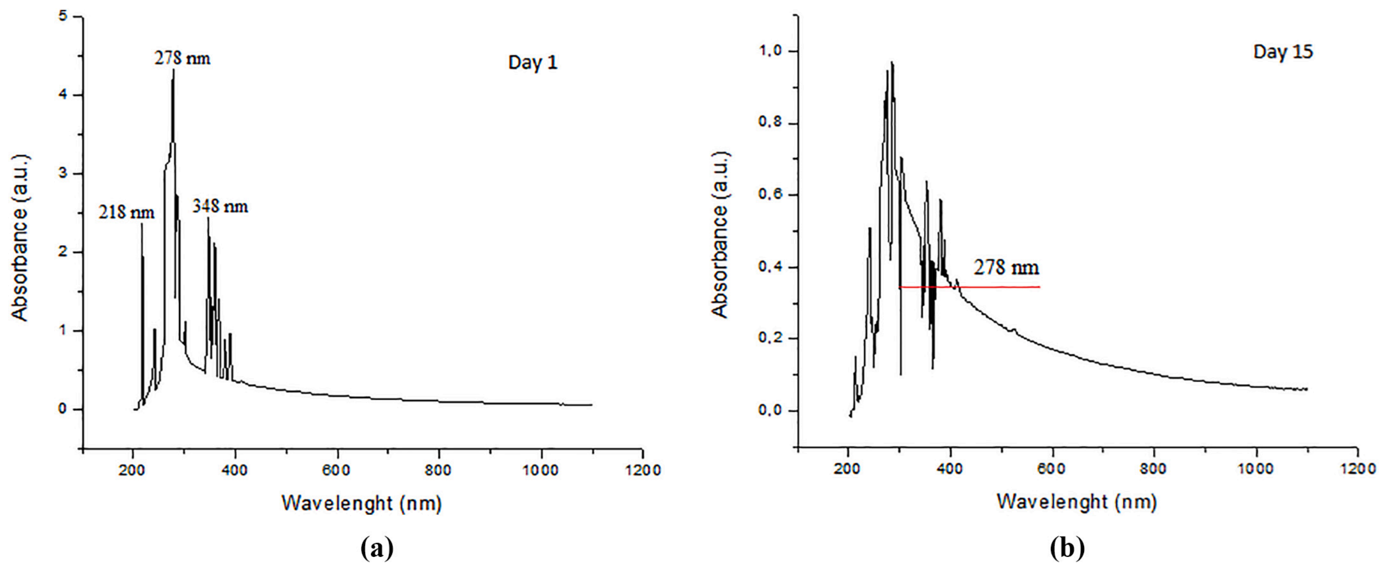

Fig. 12. The absorbance value of Al_2O_3-POE nanolubricants with 40 min sonication (a) day 1 (b) and day 15.

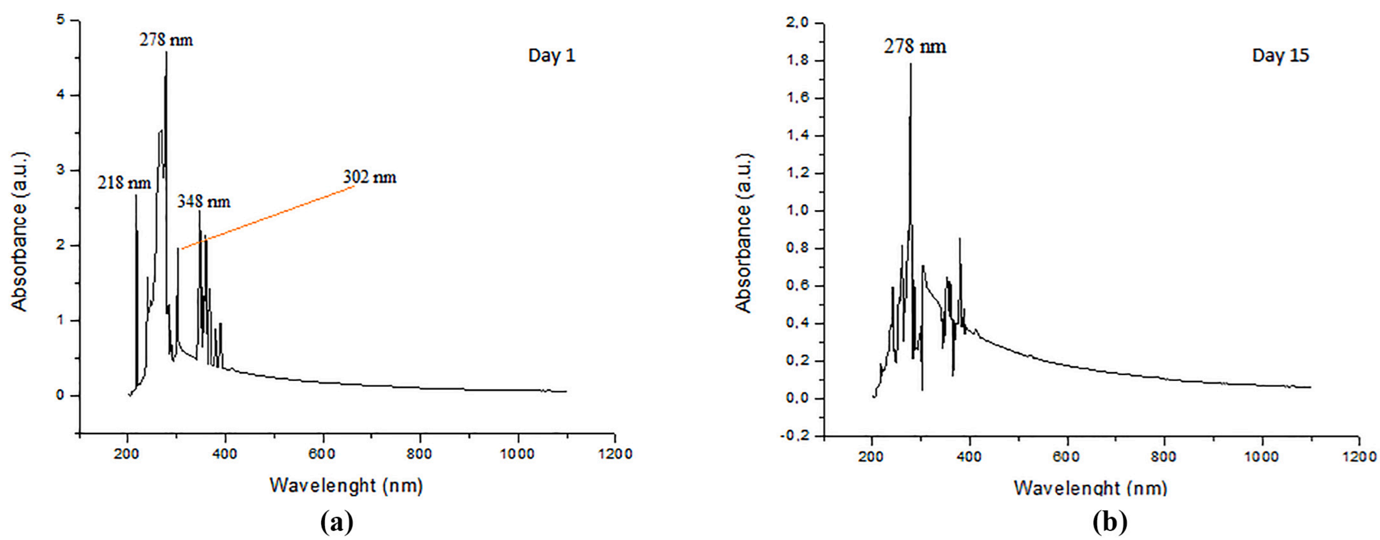

Fig. 13. The absorbance value of Al_2O_3-POE nanolubricants with 60 min sonication on (a) Day 1 (b) and Day 15.

scan's outcome and the absorbance of the Al_2O_3-POE nanolubricants on day 15. It can be seen that the absorbance decreases in each sample and that there is an increase in agglomeration.

Further analysis regarding the absorbance ratio of this present work will be more elaborated in the next section. To compare the stability of the nanolubricants, the researchers previously considered two key factors: (i) the selection of the most prominent absorbance peaks among the wavelength peaks that had been scanned and (ii) the selection of the absorbance peak at the shortest wavelength position [88]. According to these two factors, the wavelength of 278 nm was chosen as the reference point for evaluating the stability of the nanolubricants in the next UV visible assessment.

Fig. 11a demonstrates the relationship between the wavelength and the absorbance value of the nanolubricants Al_2O_3-POE that is not treated with ultrasound. There is a slight increase in absorbance from scanning at a wavelength of 1200–370 nm. The absorbance value appears to increase by 368 nm after passing through the wavelength. There are three major absorbance value peaks, respectively 2450, 4114, and 2102 absorbance units, each at 348 nm, 278 nm, and 218 nm. Meanwhile, Fig. 11b is the relationship between the absorbance values of the Al_2O_3-POE nanolubricants on day 15. There is a decrease in the significant spectra 1.165, 3.760, and 1.020. The highest decrease occurs in a wavelength of 278 nm, which is 91%. It is significantly dropped since this sample does not get any treatment of sonication.

These three peaks and other small peaks show the absorbance values. It also illustrates how large the nanoparticles absorb the particular light spectrum in the nanolubricants. While the number of peaks also shows the number of agglomeration and aggregation of nanoparticles in the nanolubricants.

The major three peaks and others reflect the absorbance values of the nanolubricants. These peaks also demonstrate how often nanoparticles can absorb the light that reaches them in the nanolubricants. The number of peaks on the graph also indicates the amount of agglomeration and aggregation, as reported by Xian et al. [87]. Both agglomeration and aggregation occur in the nanolubricants due to the attractive forces between the nanoparticle atomic bonding upon its nanolubricants due to Van der Walls forces, as Jiang et al., [76] and Mahbubul et al. [89] stated. The result of the Al_2O_3-POE nanolubricants ultrasonic treatment procedure for 40 min is shown in Fig. 12a and b.

Based on the graph in Fig. 12a, the similar pattern as Fig. 12b

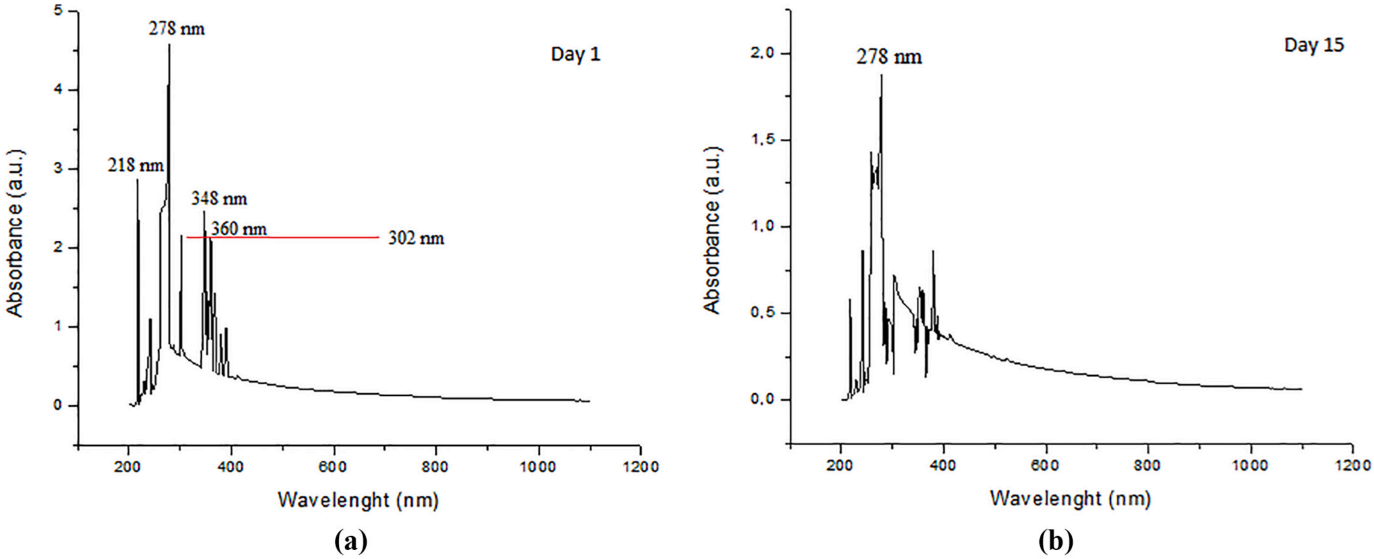

Fig. 14. The absorbance value of Al_2O_3-POE nanolubricants with 80 min sonication on (a) day one and (b) on day 15.

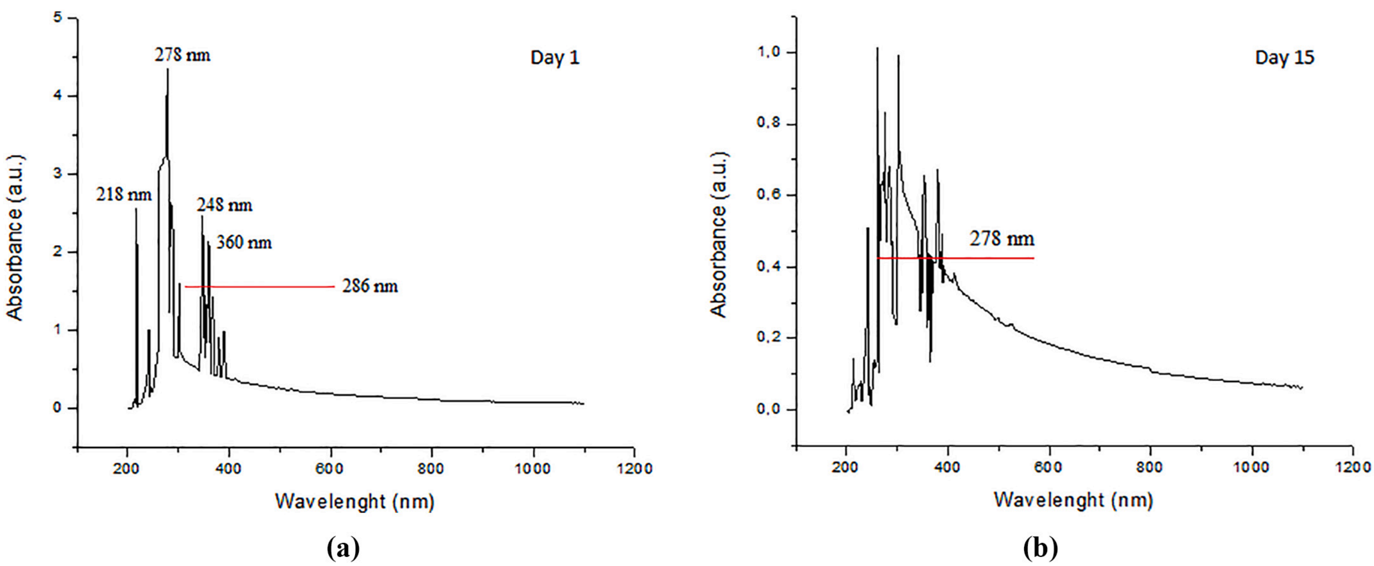

Fig. 15. The absorbance value of Al_2O_3-POE nanolubricants with 100 min sonication on (a) day one and (b) day 15.

remains the same. There has been an insignificant rise in absorption from the initial scan point at 1100–200 nm. There are three significant peaks at 348 nm, 278 nm, and 218 nm, with absorbance values at 2.456, 4.326, and 2383, respectively. It can be seen that the absorbance values at these three points are typically increased. The wavelength 278 nm is the highest peak compared with the UV visible assessment in Day 15, as shown in Fig. 12b. It indicates decreased absorbance value in wavelength 278 nm to 0.536. Meaning, the absorbance value of sample 2's UV visible result is dropped by 3.79 absorbance unit or 87.6%. Fig. 13a shows the absorbance value of Al2O3-POE nanolubricants that has been treated with sonication for 60 min on day 1. The absorbance value of the highest peak is 4.579, which is shown on 278 wavelengths. On day 15, the absorbance value drops to 1.789. Thus, there is a 60% decrease in absorbance value. A 60-min-treatment was able to boost the amount of light absorption and increase the amount of agglomeration that occurred in the nanolubricants.

Fig. 14a shows five significant peaks, i.e. peak at wavelengths of 360 nm, 348 nm, 302 nm, 278 nm, and 218 nm, with each absorbance value being 2142, 2464, 2153, 4582, and 2873, respectively. However, there are several other peaks in other areas that demonstrate the absorbance capacity of the nanolubricants. Some of these peaks do not draw attention because they are not dominant even if the location is in the longer wavelength.

The absorbance value at the highest wavelength at 278 nm is 1.882. Thus, there is a decrease in the absorbance value of 58.9%. Based on Fig. 15a, there are five absorbance peaks considered. They are at the wavelength of 360 nm, 348 nm, 286 nm, 278 nm, and 218 nm. The values for each wavelength are 2.148, 2.474, 2.644, 4.352, and 2.562. The absorbance value at the maximum wavelength at 278 nm is 0.468. Thus, there is an 89.2% drop in absorbance value. Fig. 16a shows the absorbance value of the nanolubricants Al_2O_3-POE. The nanolubricants was ultrasonicated for 120 min on day one and day 15 (Fig. 16b). A dramatic decrease at a wavelength of 278 nm is 3042. The absorbance value drops significantly at the wavelength of 348 and 218 by 1213 and 1429, respectively. Major agglomeration occurs in the wavelength ranged between 400 and 358 nm after 15 days, as shown in Fig. 16b. The absorbance value, at the maximum wavelength at 278 nm, is 0.468. Thus, there is a drop of 88.3% of absorbance value. This decline can be

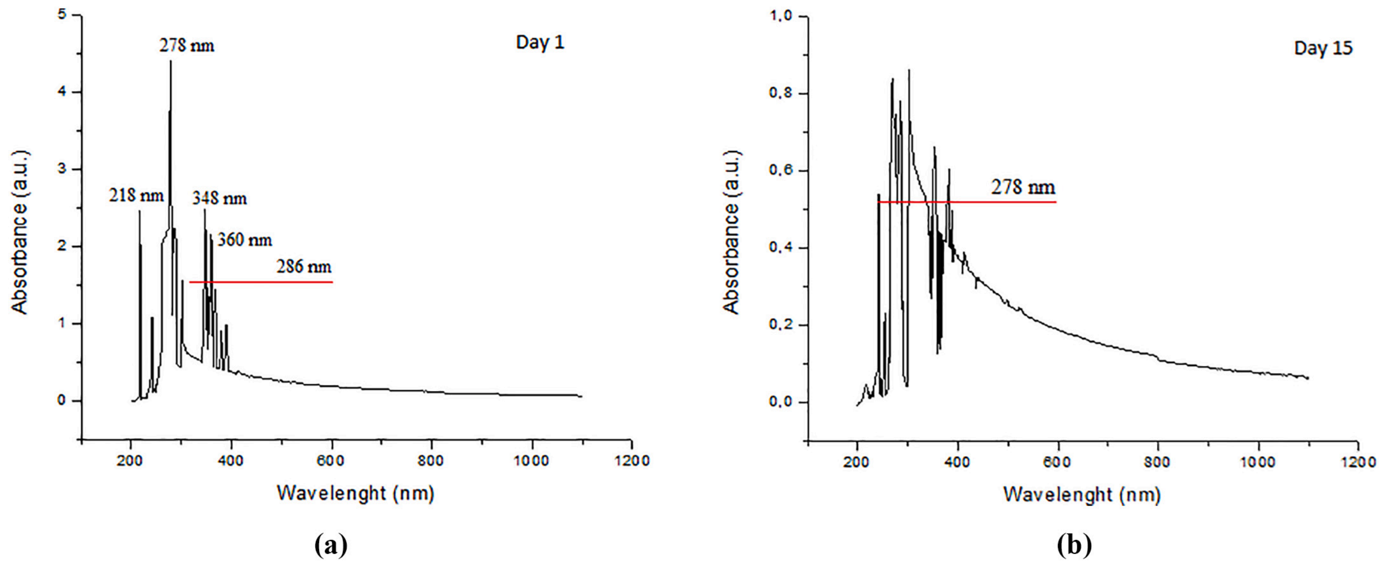

Fig. 16. The absorbance value of Al_2O_3-POE nanolubricants with 120 min sonication on (a) day one and (b) day 15.

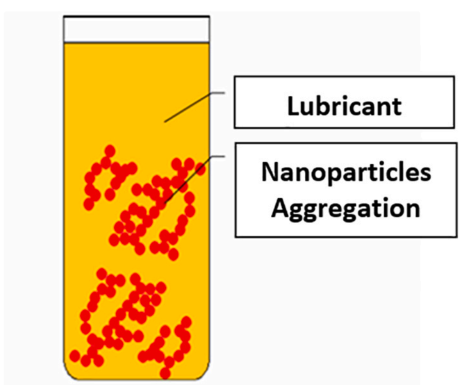

Fig. 17. Nanoparticle aggregation illustration in lubricant.

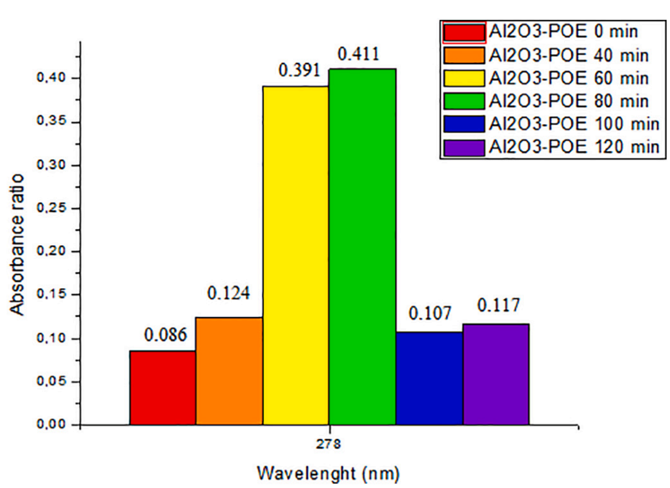

Fig. 18. Absorbance ratio of each Al_2O_3-POE nanolubricants sample.

argued due to the intense attraction between nanoparticles at the atomic level. The intense attraction generates agglomeration and aggregation of nanoparticles in the lubricant, as illustrated in Fig. 17.

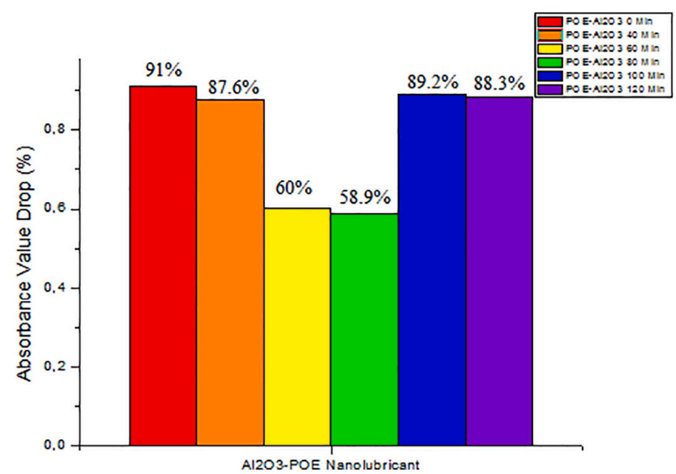

Fig. 19. Absorbance value drop percentage in every Al_2O_3-POE nanolubricants sample.

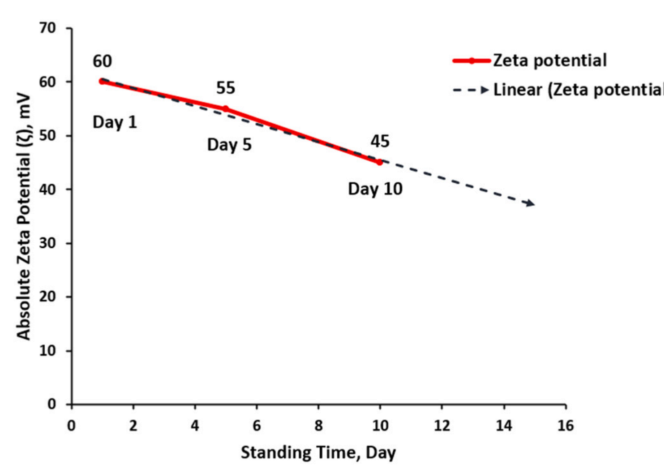

Fig. 20. Absolute Zeta Potential of Al_2O_3-POE nanolubricant as a function of time.

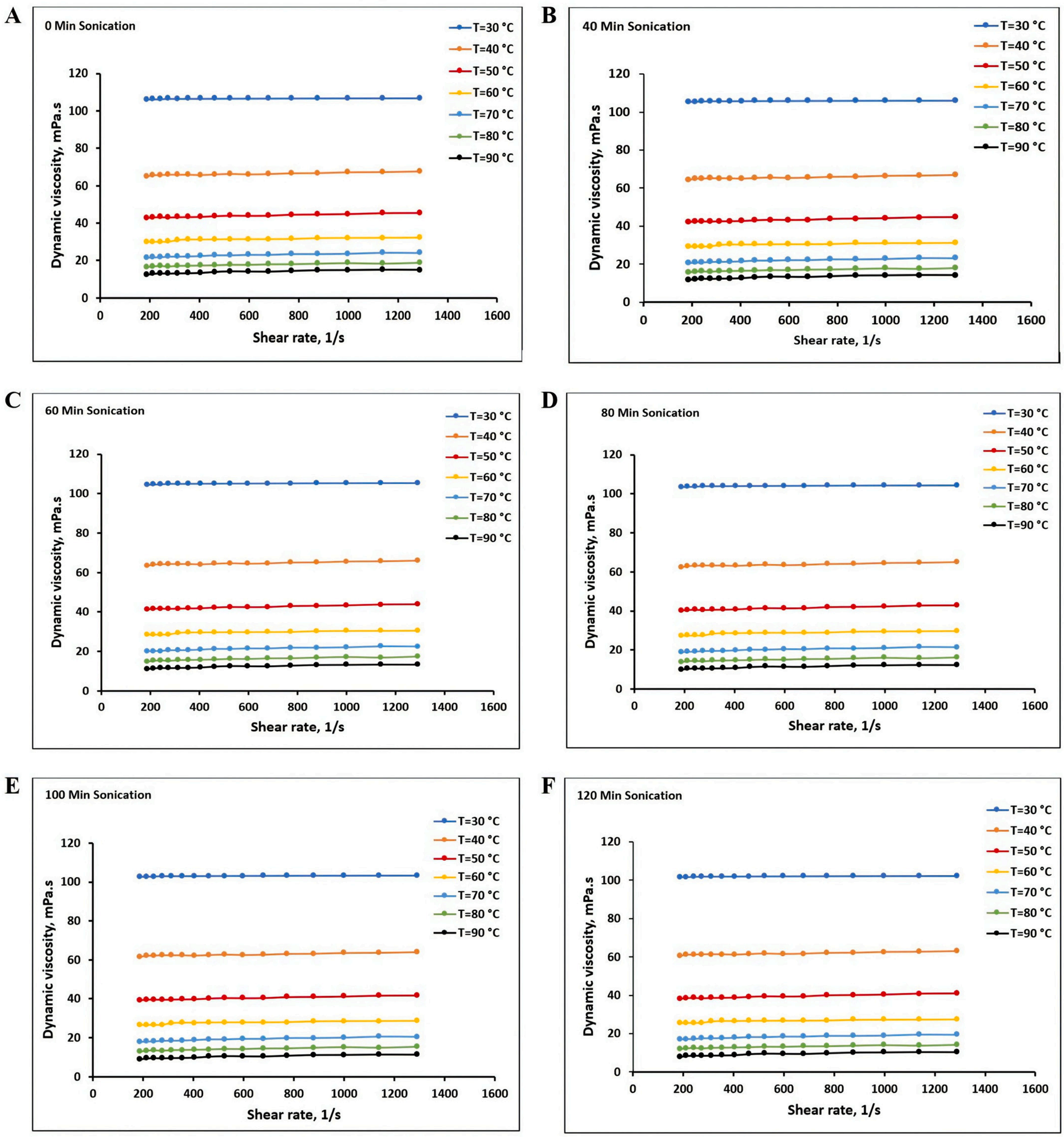

Fig. 21. **(a)** 0 min sonication duration effect on dynamic viscosity at different shear rate. **(b)** 40 min sonication duration effect on dynamic viscosity at different shear rate. **(c)** 60 min sonication duration effect on dynamic viscosity at different shear rate. **(d)** 80 min sonication duration effect on dynamic viscosity at different shear rate. **(e)** 100 min sonication duration effect on dynamic viscosity at different shear rate. **(f)** 120 min sonication duration effect on dynamic viscosity.

3.5. Absorbance ratio of Al_2O_3-POE Nanolubricants studies

The absorbance ratio method is a simultaneous measurement method for two components with an absorbance ratio at any two wavelengths. It is a constant value regardless of the concentration or the length of the wavelength. Previous researchers have used this standard method to determine the stability of nanolubricants analytically. Picking the highest peak at the shortest wavelength based on the nanolubricants scan data of Al_2O_3-POE in each sample [90,91]. The absorbance ratio (A_r) is defined as that initial absorbance (A) is over final absorbance (A_0), as shown in Eq. (2).

$$A_r = \frac{A}{A_0} \tag{2}$$

Fig. 18 shows the absorbance ratio of each Al_2O_3-POE nanolubricants sample by comparing the highest peak absorbance value at a wavelength

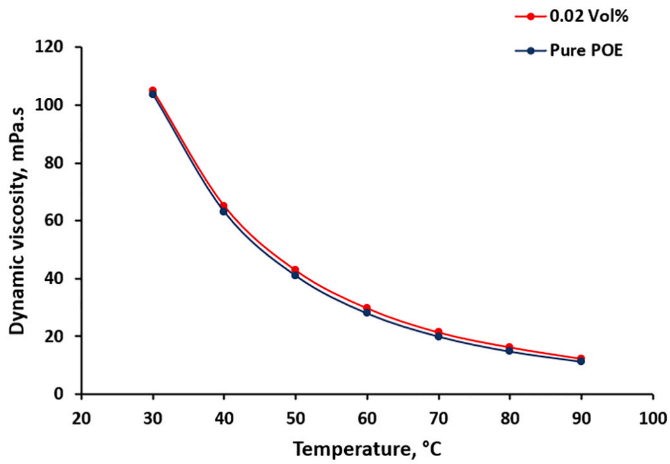

Fig. 22. Dynamic viscosity of Al_2O_3-POE nanolubricants and POE lubricants at different temperature.

of 278 nm. Al_2O_3-POE nanolubricants were treated for 60 and 80 min. The nanolubricants had a higher absorbance than the other samples. As a result of this treatment, the absorbance ratio is 0.391 and 0.411, respectively. This phenomenon confirms the visual observation conducted, as shown in Fig. 7b. It shows the stability of the Al_2O_3-POE nanolubricants sample.

The other four samples have a low absorbance ratio due to a high degree of agglomeration, accumulation, and sedimentation. Besides, it can be argued that the high agglomeration, aggregation, and sedimentation of Al_2O_3-POE is because Al_2O_3 is an oxide-based nanoparticle with a hydroxyl group on its surface. Thus, the Al2O3 is a naturally hydrophilic form that appears to be unstable with this type of lubricant [92,93]. Therefore, the modification of the Al_2O_3 surface is required to increase the wettability of the Al_2O_3 surface to oil, as discussed by Liu et al., [94,95].

However, for this present analysis, sample 4 is the most stable sample accompanied by sample 3 with an absorbance value of 0.411 and 0.391. In which, these two samples have the lowest absorbance value drop, as shown in Fig. 19.

3.6. Absolute zeta potential analysis

The interaction between the particles and the particle-lubricant interface over time determines the stability of the colloid system, and the stability of the Al2O3-POE nanolubricant is closely related to the density of its surface charge. As a result, after determining the results of the absorbance ratio, this stability analysis must be performed using the zeta potential measurement method to verify the stability level of the prepared nanolubricants.

The absorbance ratio's main output as shown in Fig. 20 was used as the main reference. In the zeta potential test, the sample with the highest absorbance ratio was used for further analysis as suggested by Sharif et al. [96] and Zawawi et al. [97].

Fig. 20 depicts the results of the 240-h absolute zeta potential evaluation (10 days). The measurements were taken on the first day, day 5, and day 10. The Al2O3-POE nanolubricant had a zeta potential of 60 mV on day 1, 55 mV on day 5, and 45 mV on day 10. According to the zeta potential examination, the prepared Al_2O_3-POE nanolubricant can be classified as having acceptable stability based on these findings since it ranges between 30 mV – 60 mV [98].

3.7. Various sonication duration effect on dynamic viscosity

Various sonication duration was used to prepare nanolubricants. The rheological behavior of the nanolubricant prepared without sonication is shown in Fig. 21a (0 sonication duration). Fig. 21b, c, d, e, and f demonstrate nanolubricants rheological behavior prepared by sonication for 40, 60, 80, 100, and 120 min, respectively. According to the graph, the sonication duration has no significant effect on the nanolubricant behavior. In all samples of different sonication durations, the nanolubricant behaves in Newtonian fluid. This phenomenon demonstrates that shear rate changes in each sample do not increase nanolubricant dynamic viscosity significantly. The Al_2O_3-POE dynamic viscosity graph tends to be flat with a very small increment rate.

These graphs demonstrate two Newtonian fluid behavior. Specifically, the behavior of the nanolubricant thickening viscosity, which shows a small rise in dynamic viscosity at high shear rate values and a thinning viscosity at low shear rates.

Fig. 22 depicts the effect of adding Al_2O_3 nanoparticles to a POE lubricant tested in various temperature, which results in an increase in the nanolubricant's viscosity. The dynamic viscosity increases as the nanoparticle added to the lubricant. The effect of the nanoparticle density, which is higher than the lubricant induces this phenomenon. Furthermore, this phenomenon is caused by the van der Walls force, which causes the lubricant's viscosity to increase [75]. The graph demonstrates the dynamic viscosity decreases as the temperature increased. At this stage, the presence of a small proportion of nanoparticles indicates Newtonian behavior as shown in Fig. 2, in which the viscosity is determined by the shear stress or the applied shear rate.

Shear thickening occurs at higher stresses, according to Norman et al. [99] once the critical shear stress is reached, viscosity increases rapidly and sometimes discontinuously. The presence of dynamic viscosity in the nanolubricants under our investigation contradicts our previous experimental findings. Even though there is shear thickening at higher shear stresses and rates. Viscosity appears to level off at much higher shear rates. The viscosity will start to rise above a certain shear-rate threshold [100]. However, the graphs depict that the dynamic viscosity does not increase rapidly and significantly, as shown in Fig. 21. As a result, this nanolubricant's behavior can be classified as Newtonian fluid [101].

4. Conclusions

According to the results of the assessment that had been carried out, a range of essential points can be drawn as follow:

The influence of sonication duration leads to the stability of the Al_2O_3-POE nanolubricants. The stability is determined by the absorbance value and the absorbance ratio of the Al_2O_3-POE nanolubricants. Every sample has a maximum drop on the 15th day with an absorbance ratio range of 58.9% and 91%.

In this study, the interlude sonication period gives the most optimal impact at 80-min sonication. The highest absorbance ratio evidences it among other samples, which is 0.411, and the lowest drop absorbance value, which is 58.9%. The absolute zeta potential evaluation result for 240 h is 45 mV. The Al_2O_3-POE Nanolubricant was found to have an acceptable degree of stability within the examination period.

Agglomeration, aggregation, and sedimentation are three parameters that reduce the absorbance value of nanolubricants. This state is due to Van der Walls' attraction between the elements of alumina at the atomic level. This attractive force makes two or more atoms together form a single atomic unit cell and tends to fall, ultimately creating Al_2O_3 sedimentation at the bottom of the experimental tube.

The various sonication duration on Al_2O_3-POE nanolubricants does not give signification enhancement on dynamic viscosity. Even though there is shear thickening at higher shear stresses and rates. The dynamic viscosity slightly appears to level up at much higher shear rates. Thus, the rheological behavior of Al_2O_3-POE nanolubricants show Newtonian behavior in all examined samples.

Another element that stimulates the instability of the Al_2O_3-POE nanolubricants is the surface of Al_2O_3 itself. Al_2O_3 is an oxide-based nanoparticle with many hydroxyls groups on its surface. This state allows Al_2O_3 to become a hydrophilic compound that is hardly stable for an extended period when combined with oil-based fluid. An active treatment such as a functionalization nanoparticles surface modification should be performed to Al_2O_3 for future investigation. The surface modification leads to the Al_2O_3's surface wettability enhancement when it disperses into the lubricant.

Authorship statement

All persons who meet authorship criteria are listed as authors, and all authors certify that they have participated sufficiently in the work to take public responsibility for the content, including participation in the concept, design, analysis, writing, or revision of the manuscript. Furthermore, each author certifies that this material or similar material has not been and will not be submitted to or published in any other publication before its appearance in the International Communications in Heat and Mass Transfer.

Declaration of Competing Interest

The authors declare that they have not known competing for financial interests or personal relationships that could have influenced the work reported in this paper.

Acknowledgements

This research was funded by Ningxia University, China under Helan Mountain Scholars scheme. The authors are also grateful to Universiti Malaysia Pahang (UMP) for the financial support given under the internal research fund RDU 190336 and FRGS grant RDU 1901112.

References

[1] J. Rajaguru, N. Arunachalam, A comprehensive investigation on the effect of flood and MQL coolant on the machinability and stress corrosion cracking of super duplex stainless steel, J. Mater. Process. Technol. 276 (2020) 116417, https://doi.org/10.1016/j.jmatprotec.2019.116417.
[2] S.C. Pang, M.A. Kalam, H.H. Masjuki, M.A. Hazrat, A review on air flow and coolant flow circuit in vehicles' cooling system, Int. J. Heat Mass Transf. 55 (2012) 6295–6306, https://doi.org/10.1016/j.ijheatmasstransfer.2012.07.002.
[3] Y. Deng, C. Feng, J. E, H. Zhu, J. Chen, M. Wen, H. Yin, Effects of different coolants and cooling strategies on the cooling performance of the power lithium ion battery system: a review, Appl. Therm. Eng. 142 (2018) 10–29, https://doi.org/10.1016/j.applthermaleng.2018.06.043.
[4] K. Golec, E.C. Hill, P. Kazemi, R.O. Skold, Oil / water partition for some hydroxyalkylamines and antimicrobial efficacy in metalworking coolants, Trinology Int. (1989) 375–382.
[5] N. Sandeep, A. Malvandi, Enhanced heat transfer in liquid thin film flow of non-Newtonian nanofluids embedded with graphene nanoparticles, Adv. Powder Technol. 27 (2016) 2448–2456, https://doi.org/10.1016/j.apt.2016.08.023.
[6] A.A.M. Redhwan, W.H. Azmi, M.Z. Sharif, F.Y. Hagos, Development of nanolubricant automotive air conditioning (AAC) test rig, MATEC Web Conf. 90 (2016), https://doi.org/10.1051/matecconf/20179001050.
[7] G. Ding, H. Peng, W. Jiang, Y. Gao, The migration characteristics of nanoparticles in the pool boiling process of nanorefrigerant and nanorefrigerant-oil mixture, Int. J. Refrig. 32 (2009) 114–123, https://doi.org/10.1016/j.ijrefrig.2008.08.007.
[8] M.S.Y. Ebaid, A.M. Ghrair, M. Al-Busoul, Experimental investigation of cooling photovoltaic (PV) panels using (TiO2) nanofluid in water -polyethylene glycol mixture and (Al2O3) nanofluid in water- cetyltrimethylammonium bromide mixture, Energy Convers. Manag. 155 (2018) 324–343, https://doi.org/10.1016/j.enconman.2017.10.074.
[9] R. Taherialekouhi, S. Rasouli, A. Khosravi, An experimental study on stability and thermal conductivity of water-graphene oxide/aluminum oxide nanoparticles as a cooling hybrid nanofluid, Int. J. Heat Mass Transf. 145 (2019) 118751, https://doi.org/10.1016/j.ijheatmasstransfer.2019.118751.
[10] R.D. Jilte, R. Kumar, M.H. Ahmadi, Cooling performance of nanofluid submerged vs. nanofluid circulated battery thermal management systems, J. Clean. Prod. 240 (2019), https://doi.org/10.1016/j.jclepro.2019.118131.
[11] C.J. Ho, J.C. Liao, C.H. Li, W.M. Yan, M. Amani, Experimental study of cooling performance of water-based alumina nanofluid in a minichannel heat sink with MEPCM layer embedded in its ceiling, Int. Commun. Heat Mass Transf. 103 (2019) 1–6, https://doi.org/10.1016/j.icheatmasstransfer.2019.02.001.
[12] Ç.V. Yıldırım, Experimental comparison of the performance of nanofluids, cryogenic and hybrid cooling in turning of Inconel 625, Tribol. Int. 137 (2019) 366–378, https://doi.org/10.1016/j.triboint.2019.05.014.
[13] M.K.A. Ali, H. Xianjun, Improving the heat transfer capability and thermal stability of vehicle engine oils using Al2O3/TiO2 nanomaterials, Powder Technol. 363 (2020) 48–58, https://doi.org/10.1016/j.powtec.2019.12.051.
[14] T.A. Alkanhal, M. Sheikholeslami, M. Usman, R. ul Haq, A. Shafee, A.S. Al-Ahmadi, I. Tlili, Thermal management of MHD nanofluid within the porous medium enclosed in a wavy shaped cavity with square obstacle in the presence of radiation heat source, Int. J. Heat Mass Transf. 139 (2019) 87–94, https://doi.org/10.1016/j.ijheatmasstransfer.2019.05.006.
[15] K.J. Chua, S.K. Chou, W.M. Yang, J. Yan, A comprehensive review on mixed convection of nanofluids in various shapes of enclosures, Powder Technol. 343 (2019) 880–907, https://doi.org/10.1016/j.powtec.2018.11.006.
[16] K. Abdul Hamid, W.H. Azmi, R. Mamat, K.V. Sharma, Heat transfer performance of TiO2–SiO2 nanofluids in a tube with wire coil inserts, Appl. Therm. Eng. 152 (2019) 275–286, https://doi.org/10.1016/j.applthermaleng.2019.02.083.
[17] H. Masuda, A. Ebata, K. Teramae, N. Hishinuma, Alteration of thermal conductivity and viscosity of liquid by dispersing ultra-fine particles. Dispersion of Al2O3, SiO2 and TiO2 ultra-fine particles, Netsu Bussei. 7 (1993) 227–233, https://doi.org/10.2963/jjtp.7.227.
[18] S.U.S. Choi, Enhancing thermal conductivity of fluids with nanoparticles, Am. Soc. Mech. Eng. Fluids Eng. Div. FED. 231 (1995) 99–105.
[19] I. Elbadawy, M. Fayed, Reliability of Al2O3 nanofluid concentration on the heat transfer augmentation and resizing for single and double stack microchannels, Alexandria Eng. J. 59 (2020) 1771–1785, https://doi.org/10.1016/j.aej.2020.04.046.
[20] W. Yu, D.M. France, J.L. Routbort, S.U.S. Choi, Review and comparison of nanofluid thermal conductivity and heat transfer enhancements, Heat Transf. Eng. 29 (2008) 432–460, https://doi.org/10.1080/01457630701850851.
[21] M.U. Sajid, H.M. Ali, Thermal conductivity of hybrid nanofluids: a critical review, Int. J. Heat Mass Transf. 126 (2018) 211–234, https://doi.org/10.1016/j.ijheatmasstransfer.2018.05.021.
[22] B. Buonomo, O. Manca, L. Marinelli, S. Nardini, Effect of temperature and sonication time on nanofluid thermal conductivity measurements by nano-flash method, Appl. Therm. Eng. 91 (2015) 181–190, https://doi.org/10.1016/j.applthermaleng.2015.07.077.
[23] R. Gangadevi, B.K. Vinayagam, S. Senthilraja, Effects of sonication time and temperature on thermal conductivity of CuO/water and Al2O3/water nanofluids with and without surfactant, Mater. Today Proc. 5 (2018) 9004–9011, https://doi.org/10.1016/j.matpr.2017.12.347.
[24] Z. Chen, A. Shahsavar, A.A.A.A. Al-Rashed, M. Afrand, The impact of sonication and stirring durations on the thermal conductivity of alumina-liquid paraffin nanofluid: an experimental assessment, Powder Technol. 360 (2019) 1134–1142, https://doi.org/10.1016/j.powtec.2019.11.036.
[25] A. Asadi, F. Pourfattah, I. Miklós Szilágyi, M. Afrand, G. Żyła, H. Seon Ahn, S. Wongwises, H. Minh Nguyen, A. Arabkoohsar, O. Mahian, Effect of sonication characteristics on stability, thermophysical properties, and heat transfer of nanofluids: a comprehensive review, Ultrason. Sonochem. 58 (2019), https://doi.org/10.1016/j.ultsonch.2019.104701.
[26] L. Li, Y. Zhai, Y. Jin, J. Wang, H. Wang, M. Ma, Stability, thermal performance and artificial neural network modeling of viscosity and thermal conductivity of Al2O3-ethylene glycol nanofluids, Powder Technol. 363 (2020) 360–368, https://doi.org/10.1016/j.powtec.2020.01.006.
[27] M.M. Ghafurian, Z. Akbari, H. Niazmand, R. Mehrkhah, S. Wongwises, O. Mahian, Effect of sonication time on the evaporation rate of seawater containing a nanocomposite, Ultrason. Sonochem. 61 (2020) 104817, https://doi.org/10.1016/j.ultsonch.2019.104817.
[28] I. Zarma, M. Ahmed, S. Ookawara, Enhancing the performance of concentrator photovoltaic systems using nanoparticle-phase change material heat sinks, Energy Convers. Manag. 179 (2019) 229–242, https://doi.org/10.1016/j.enconman.2018.10.055.
[29] M.A. Kedzierski, Effect of Al2O3 nanolubricant on R134a pool boiling heat transfer, Int. J. Refrig. 34 (2011) 498–508, https://doi.org/10.1016/j.ijrefrig.2010.10.007.
[30] E. Nourafkan, M. Asachi, H. Jin, D. Wen, W. Ahmed, Stability and photo-thermal conversion performance of binary nanofluids for solar absorption refrigeration systems, Renew. Energy 140 (2019) 264–273, https://doi.org/10.1016/j.renene.2019.01.081.
[34] N. Amira, R. Nazar, K. Naganthran, I. Pop, Stability analysis of MHD hybrid nanofluid flow over a stretching / shrinking sheet with quadratic velocity, Alexandria Eng. J. 60 (2021) 915–926, https://doi.org/10.1016/j.aej.2020.10.020.
[35] S. Aberoumand, A. Jafarimoghaddam, Tungsten (III) oxide (WO3) – silver / transformer oil hybrid nanofluid: preparation, stability, thermal conductivity and dielectric strength, Alexandria Eng. J. 57 (2018) 169–174, https://doi.org/10.1016/j.aej.2016.11.003.
[36] N.R. Karthikeyan, J. Philip, B. Raj, Effect of clustering on the thermal conductivity of nanofluids, Mater. Chem. Phys. 109 (2008) 50–55, https://doi.org/10.1016/j.matchemphys.2007.10.029.
[37] C. Gu, Q. Li, Z. Gu, G. Zhu, Study on application of CeO2 and CaCO3 nanoparticles in lubricating oils, J. Rare Earths 26 (2008) 163–167, https://doi.org/10.1016/S1002-0721(08)60058-7.
[38] M.S. Liu, M. Ching-Cheng Lin, I. Te Huang, C.C. Wang, Enhancement of thermal conductivity with carbon nanotube for nanofluids, Int. Commun. Heat Mass Transf. 32 (2005) 1202–1210, https://doi.org/10.1016/j.icheatmasstransfer.2005.05.005.
[39] C. Pang, J.Y. Jung, J.W. Lee, Y.T. Kang, Thermal conductivity measurement of methanol-based nanofluids with Al2O3 and SiO2 nanoparticles, Int. J. Heat Mass

Transf. 55 (2012) 5597–5602, https://doi.org/10.1016/j.ijheatmasstransfer.2012.05.048.
[40] B. Ruan, A.M. Jacobi, Ultrasonication effects on thermal and rheological properties of carbon nanotube suspensions, Nanoscale Res. Lett. 7 (2012) 1–14, https://doi.org/10.1186/1556-276X-7-127.
[41] A. Asadi, M. Asadi, M. Siahmargoi, T. Asadi, M. Gholami Andarati, The effect of surfactant and sonication time on the stability and thermal conductivity of water-based nanofluid containing mg(OH) 2 nanoparticles: an experimental investigation, Int. J. Heat Mass Transf. 108 (2017) 191–198, https://doi.org/10.1016/j.ijheatmasstransfer.2016.12.022.
[42] L. Ali, Z. Omar, I. Khan, A.H. Seikh, E.M. Sherif, K. Sooppy, Stability analysis and multiple solution of Cu – Al2O3/H2O nanofluid contains hybrid nanomaterials over a shrinking surface in the presence of viscous dissipation, Integr. Med. Res. (2019) 1–12, https://doi.org/10.1016/j.jmrt.2019.10.071.
[43] A. Mohammed, N. Azwadi, C. Sidik, W. Azmi, W. Hamzah, R. Mamat, An experimental determination of thermal conductivity and electrical conductivity of bio glycol based Al2O3 nano fl uids and development of new correlation, Int. Commun. Heat Mass Transf. 73 (2016) 75–83, https://doi.org/10.1016/j.icheatmasstransfer.2016.02.006.
[44] M.F. Nabil, W.H. Azmi, K. Abdul Hamid, R. Mamat, F.Y. Hagos, An experimental study on the thermal conductivity and dynamic viscosity of TiO2-SiO2 nanofluids in water: ethylene glycol mixture, Int. Commun. Heat Mass Transf. 86 (2017) 181–189, https://doi.org/10.1016/j.icheatmasstransfer.2017.05.024.
[45] A.M. Sadoun, M.M. Mohammed, E.M. Elsayed, A.F. Meselhy, O.A. El-Kady, Effect of nano Al2O3 coated Ag addition on the corrosion resistance and electrochemical behavior of Cu-Al2O3 nanocomposites, J. Mater. Res. Technol. 9 (2020) 4485–4493, https://doi.org/10.1016/j.jmrt.2020.02.076.
[46] A.M. Sadoun, I.M.R. Najjar, M.S. Abd-Elwahed, A. Meselhy, Experimental study on properties of Al–Al2O3 nanocomposite hybridized by graphene nanosheets, J. Mater. Res. Technol. 9 (2020) 14708–14717, https://doi.org/10.1016/j.jmrt.2020.10.011.
[47] A. Fathy, A. Abu-Oqail, A. Wagih, Improved mechanical and wear properties of hybrid Al-Al2O3/GNPs electro-less coated Ni nanocomposite, Ceram. Int. 44 (2018) 22135–22145, https://doi.org/10.1016/j.ceramint.2018.08.326.
[48] A.M. Sadoun, A. Fathy, Experimental study on tribological properties of cu–Al2O3 nanocomposite hybridized by graphene nanoplatelets, Ceram. Int. 45 (2019) 24784–24792, https://doi.org/10.1016/j.ceramint.2019.08.220.
[49] E. Soleimani, N. Zamani, Surface modification of alumina nanoparticles: a dispersion study in organic media, Acta Chim. Slov. 64 (2017) 644–653, https://doi.org/10.17344/acsi.2017.3459.
[50] R. Mahbubul, M.A. Saidur, Amalina, influence of particle concentration and temperature on thermal conductivity and viscosity of Al2O3/R141b nanorefrigerant, Int. Commun. Heat Mass Transf. 43 (2013) 100–104, https://doi.org/10.1016/j.icheatmasstransfer.2013.02.004.
[51] P.K. Das, A.K. Mallik, R. Ganguly, A.K. Santra, Synthesis and characterization of TiO2-water nanofluids with different surfactants, Int. Commun. Heat Mass Transf. 75 (2016) 341–348, https://doi.org/10.1016/j.icheatmasstransfer.2016.05.011.
[52] A.M. Elsaid, Experimental study on the heat transfer performance and friction factor characteristics of Co3O4 and Al2O3 based H2O/(CH2OH)2 nanofluids in a vehicle engine radiator, Int. Commun. Heat Mass Transf. 108 (2019) 104263, https://doi.org/10.1016/j.icheatmasstransfer.2019.05.009.
[53] N.N.M. Zawawi, W.H. Azmi, A.A.M. Redhwan, M.Z. Sharif, K.V. Sharma, Thermo-physical properties of Al2O3-SiO2/PAG composite nanolubricant for refrigeration system, Int. J. Refrig. 80 (2017) 1–10, https://doi.org/10.1016/j.ijrefrig.2017.04.024.
[54] A.M. Sadoun, A. Fathy, A. Abu-Oqail, H.T. Elmetwaly, A. Wagih, Structural, mechanical and tribological properties of cu–ZrO2/GNPs hybrid nanocomposites, Ceram. Int. 46 (2020) 7586–7594, https://doi.org/10.1016/j.ceramint.2019.11.258.
[55] A.M. Sadoun, A. Wagih, A. Fathy, A.R.S. Essa, Effect of tool pin side area ratio on temperature distribution in friction stir welding, Res. Phys. 15 (2019) 102814, https://doi.org/10.1016/j.rinp.2019.102814.
[56] M.S. Abd-Elwahed, A.F. Meselhy, Experimental investigation on the mechanical, structural and thermal properties of cu–ZrO2 nanocomposites hybridized by graphene nanoplatelets, Ceram. Int. 46 (2020) 9198–9206, https://doi.org/10.1016/j.ceramint.2019.12.172.
[57] K.A.E.-A.& A.F. D. SABER, Corrosion behavior of copper–alumina nanocomposites in different corrosive media, Int. J. Mech. Eng. 5 (2016) 1–10. http://www.iaset.us/view_archives.php?year=2016&id=67&jtype=2&page=3.
[58] A. Abu-Oqail, A. Samir, A.R.S. Essa, A. Wagih, A. Fathy, Effect of GNPs coated Ag on microstructure and mechanical properties of Cu-Fe dual-matrix nanocomposite, J. Alloys Compd. 781 (2019) 64–74, https://doi.org/10.1016/j.jallcom.2018.12.042.
[59] A. Wagih, A. Abu-Oqail, A. Fathy, Effect of GNPs content on thermal and mechanical properties of a novel hybrid Cu-Al2O3/GNPs coated Ag nanocomposite, Ceram. Int. 45 (2019) 1115–1124, https://doi.org/10.1016/j.ceramint.2018.10.001.
[60] A.G.N. Sofiah, M. Samykano, S. Shahabuddin, K. Kadirgama, A.K. Pandey, A comparative experimental study on the physical behavior of mono and hybrid RBD palm olein based nanofluids using CuO nanoparticles and PANI nanofibers, Int. Commun. Heat Mass Transf. 120 (2021) 105006, https://doi.org/10.1016/j.icheatmasstransfer.2020.105006.
[61] R.R. Sahoo, V. Kumar, Development of a new correlation to determine the viscosity of ternary hybrid nanofluid, Int. Commun. Heat Mass Transf. 111 (2020) 104451, https://doi.org/10.1016/j.icheatmasstransfer.2019.104451.
[62] R. Pourrajab, A. Noghrehabadi, M. Behbahani, Development of Cu/mesoporous SBA-15 nanocomposite in ethylene glycol for thermal conductivity enhancement: heat transfer applications, Int. Commun. Heat Mass Transf. 119 (2020) 104931, https://doi.org/10.1016/j.icheatmasstransfer.2020.104931.
[63] A. Ali, S.U. Ilyas, S. Garg, M. Alsaady, K. Maqsood, R. Nasir, A. Abdulrahman, M. Zulfiqar, A. Bin Mahfouz, A. Ahmed, S. Ridha, Dynamic viscosity of Titania nanotubes dispersions in ethylene glycol/water-based nanofluids: experimental evaluation and predictions from empirical correlation and artificial neural network, Int. Commun. Heat Mass Transf. 118 (2020) 104882, https://doi.org/10.1016/j.icheatmasstransfer.2020.104882.
[64] W. Ahmed, Z.Z. Chowdhury, S.N. Kazi, M.R. Johan, N. Akram, C.S. Oon, Effect of ZnO-water based nanofluids from sonochemical synthesis method on heat transfer in a circular flow passage, Int. Commun. Heat Mass Transf. 114 (2020), https://doi.org/10.1016/j.icheatmasstransfer.2020.104591.
[65] J. Alsarraf, O. Malekahmadi, A. Karimipour, I. Tlili, A. Karimipour, M. Ghashang, Increase thermal conductivity of aqueous mixture by additives graphene nanoparticles in water via an experimental/numerical study: synthesise, characterization, conductivity measurement, and neural network modeling, Int. Commun. Heat Mass Transf. 118 (2020) 104864, https://doi.org/10.1016/j.icheatmasstransfer.2020.104864.
[66] S.U. Ilyas, M. Narahari, J.T.Y. Theng, R. Pendyala, Experimental evaluation of dispersion behavior, rheology and thermal analysis of functionalized zinc oxide-paraffin oil nanofluids, J. Mol. Liq. 294 (2019), https://doi.org/10.1016/j.molliq.2019.111613.
[67] A. Nugroho, R. Basyirun, J.P. Mamat, D. Widjanarko Siregar, Ramelan, Microstructure and physical of Al2O3 2SiO4 2H2O kaolinite particle analysis by shacking time and powder metallurgy, Sci. Technol. Publ. Lda (2020) 48–53, https://doi.org/10.5220/0009006200480053.
[68] R. Pourrajab, A. Noghrehabadi, E. Hajidavalloo, M. Behbahani, Investigation of thermal conductivity of a new hybrid nanofluids based on mesoporous silica modified with copper nanoparticles: synthesis, characterization and experimental study, J. Mol. Liq. 300 (2020), https://doi.org/10.1016/j.molliq.2019.112337.
[69] A.M. Sadoun, M.M. Mohammed, A. Fathy, O.A. El-Kady, Effect of Al2O3 addition on hardness and wear behavior of Cu-Al2O3 electro-less coated Ag nanocomposite, J. Mater. Res. Technol. 9 (2020) 5024–5033, https://doi.org/10.1016/j.jmrt.2020.03.020.
[70] M.S. Abd-Elwahed, A.F. Ibrahim, M.M. Reda, Effects of ZrO2 nanoparticle content on microstructure and wear behavior of titanium matrix composite, J. Mater. Res. Technol. 9 (2020) 8528–8534, https://doi.org/10.1016/j.jmrt.2020.05.021.
[71] M. Sharifpur, A.B. Solomon, T.L. Ottermann, J.P. Meyer, Optimum concentration of nanofluids for heat transfer enhancement under cavity flow natural convection with TiO2 – water, Int. Commun. Heat Mass Transf. 98 (2018) 297–303, https://doi.org/10.1016/j.icheatmasstransfer.2018.09.010.
[72] A. Haldar, S. Chatterjee, A. Kotia, N. Kumar, S.K. Ghosh, Analysis of rheological properties of MWCNT/SiO2 hydraulic oil nanolubricants using regression and artificial neural network, Int. Commun. Heat Mass Transf. 116 (2020) 104723, https://doi.org/10.1016/j.icheatmasstransfer.2020.104723.
[73] S. Askari, A. Rashidi, H. Koolivand, Experimental investigation on the thermal performance of ultra-stable kerosene-based MWCNTs and Graphene nanofluids, Int. Commun. Heat Mass Transf. 108 (2019), https://doi.org/10.1016/j.icheatmasstransfer.2019.104334.
[74] A.S. Dalkılıç, G. Yalçın, B.O. Küçükyıldırım, S. Öztuna, A. Akdoğan Eker, C. Jumpholkul, S. Nakkaew, S. Wongwises, Experimental study on the thermal conductivity of water-based CNT-SiO2 hybrid nanofluids, Int. Commun. Heat Mass Transf. 99 (2018) 18–25, https://doi.org/10.1016/j.icheatmasstransfer.2018.10.002.
[75] S.A. Adio, M. Sharifpur, J.P. Meyer, Influence of ultrasonication energy on the dispersion consistency of Al2O3–glycerol nanofluid based on viscosity data, and model development for the required ultrasonication energy density, J. Exp. Nanosci. 11 (2016) 630–649, https://doi.org/10.1080/17458080.2015.1107194.
[76] F. Jiang, H. Sun, L. Chen, F. Lei, D. Sun, Dispersion-tribological property relationship in mineral oils containing 2D layered α-zirconium phosphate nanoplatelets, Friction. (2019), https://doi.org/10.1007/s40544-019-0294-2.
[77] V.S. Mello, E.A. Faria, S.M. Alves, C. Scandian, Enhancing Cuo nanolubricant performance using dispersing agents, Tribol. Int. 150 (2020), https://doi.org/10.1016/j.triboint.2020.106338.
[78] S. Narayanasarma, B.T. Kuzhiveli, Evaluation of the properties of POE/SiO2 nanolubricant for an energy-efficient refrigeration system – an experimental assessment, Powder Technol. 356 (2019) 1029–1044, https://doi.org/10.1016/j.powtec.2019.09.024.
[79] H. Ghodsinezhad, M. Sharifpur, J.P. Meyer, Experimental investigation on cavity flow natural convection of Al2O3–water nanofluids, Int. Commun. Heat Mass Transf. 76 (2016) 316–324, https://doi.org/10.1016/j.icheatmasstransfer.2016.06.005.
[80] S. Kim, B. Tserengombo, S.H. Choi, J. Noh, S. Huh, B. Choi, H. Chung, J. Kim, H. Jeong, Experimental investigation of heat transfer coefficient with Al2O3 nanofluid in small diameter tubes, Appl. Therm. Eng. 146 (2019) 346–355, https://doi.org/10.1016/j.applthermaleng.2018.10.001.
[81] H. Kimpton, D.A. Cristaldi, E. Stulz, X. Zhang, Thermal performance and physicochemical stability of silver nanoprism-based nanofluids for direct solar absorption, Sol. Energy 199 (2020) 366–376, https://doi.org/10.1016/j.solener.2020.02.039.
[82] A.A.M. Redhwan, W.H. Azmi, M.Z. Sharif, R. Mamat, M. Samykano, G. Najafi, Performance improvement in mobile air conditioning system using Al 2 O 3 /PAG nanolubricant, J. Therm. Anal. Calorim. 135 (2019) 1299–1310, https://doi.org/10.1007/s10973-018-7656-2.

[83] M. Atif, W.A. Farooq, A. Fatehmulla, M. Aslam, S.M. Ali, Photovoltaic and impedance spectroscopy study of screen-printed TiO2 based CdS quantum dot sensitized solar cells, Materials (Basel). 8 (2015) 355–367, https://doi.org/10.3390/ma8010355.

[84] R. Wan Hamzah, S.N.M. Azmi, K.A. Zainon, Hamid Mamat, A review on thermo-physical properties and heat transfer applications of single and hybrid metal oxide nanofluids, J. Mech. Eng. Sci. 13 (2019) 5182–5211.

[85] A. Gallego, K. Cacua, B. Herrera, D. Cabaleiro, M.M. Piñeiro, L. Lugo, Experimental evaluation of the effect in the stability and thermophysical properties of water-Al2O3 based nanofluids using SDBS as dispersant agent, Adv. Powder Technol. 31 (2020) 560–570, https://doi.org/10.1016/j.apt.2019.11.012.

[86] S. Kawai, M. Mardis, S. Machmudah, Bimetallic nanoparticle generation from Au-TiO2 film by pulsed laser ablation in an aqueous medium, Alexandria Eng. J. 60 (2021) 2225–2234, https://doi.org/10.1016/j.aej.2020.12.031.

[87] H.W. Xian, N.A.C. Sidik, R. Saidur, Impact of different surfactants and ultrasonication time on the stability and thermophysical properties of hybrid nanofluids, Int. Commun. Heat Mass Transf. 110 (2020), https://doi.org/10.1016/j.icheatmasstransfer.2019.104389.

[88] A. Ahmad, M. Amir, A.A. Alshadidi, M.D. Hussain, A. Haq, M. Kazi, Central composite design expert-supported development and validation of HPTLC method: relevance in quantitative evaluation of protopine in Fumaria indica, Saudi Pharm. J. 28 (2020) 487–494, https://doi.org/10.1016/j.jsps.2020.02.011.

[89] I.M. Mahbubul, I.M. Shahrul, S.S. Khaleduzzaman, R. Saidur, M.A. Amalina, A. Turgut, Experimental investigation on effect of ultrasonication duration on colloidal dispersion and thermophysical properties of alumina – water nanofluid, Int. J. Heat Mass Transf. 88 (2015) 73–81, https://doi.org/10.1016/j.ijheatmasstransfer.2015.04.048.

[90] G. Singh, D. Kumar, D. Sharma, M. Singh, S. Kaur, Q-Absorbance ratio spectrophotometric method for the simultaneous estimation of prednisolone and 5-amino salicylic acid in tablet dosage form, J. Appl. Pharm. Sci. 2 (2012) 222–226, https://doi.org/10.7324/JAPS.2012.2736.

[91] L. Lin, H. Peng, Z. Chang, G. Ding, Experimental investigation on TiO2 nanoparticle migration from refrigerant–oil mixture to lubricating oil during refrigerant dryout, Int. J. Refrig. 77 (2017) 75–86, https://doi.org/10.1016/j.ijrefrig.2017.02.026.

[92] A. Talavari, B. Ghanavati, A. Azimi, S. Sayyahi, Preparation and characterization of PVDF-filled MWCNT hollow fiber mixed matrix membranes for gas absorption by Al2O3 nanofluid absorbent via gas–liquid membrane contactor, Chem. Eng. Res. Des. 156 (2020) 478–494, https://doi.org/10.1016/j.cherd.2020.01.017.

[93] S.U. Ilyas, R. Pendyala, M. Narahari, L. Susin, Stability, rheology and thermal analysis of functionalized alumina- thermal oil-based nanofluids for advanced cooling systems, Energy Convers. Manag. 142 (2017) 215–229, https://doi.org/10.1016/j.enconman.2017.01.079.

[94] Z. Liu, L. Yao, X. Pan, Q. Liu, H. Huang, A green and facile approach to the efficient surface modification of alumina nanoparticles with fatty acids, Appl. Surf. Sci. 447 (2018) 664–672, https://doi.org/10.1016/j.apsusc.2018.04.035.

[95] A.O. Gbadamosi, R. Junin, M.A. Manan, A. Agi, J.O. Oseh, J. Usman, Effect of aluminium oxide nanoparticles on oilfield ploycrylamide: rheology, interfacial tension, wettebility and oil displacement studies, J. Mol. Liq. 53 (2019) 1689–1699, https://doi.org/10.1017/CBO9781107415324.004.

[96] M.Z. Sharif, W.H. Azmi, A.A.M. Redhwan, R. Mamat, Investigation of thermal conductivity and viscosity of Al2O3/PAG nanolubricant for application in automotive air conditioning system, Int. J. Refrig. 70 (2016) 93–102, https://doi.org/10.1016/j.ijrefrig.2016.06.025.

[97] N.N.M. Zawawi, W.H. Azmi, M.Z. Sharif, G. Najafi, Experimental investigation on stability and thermo-physical properties of Al2O3–SiO2/PAG nanolubricants with different nanoparticle ratios, J. Therm. Anal. Calorim. 135 (2019) 1243–1255, https://doi.org/10.1007/s10973-018-7670-4.

[98] I.M. Mahbubul, T.H. Chong, S.S. Khaleduzzaman, I.M. Shahrul, R. Saidur, B. D. Long, M.A. Amalina, Effect of ultrasonication duration on colloidal structure and viscosity of alumina-water nanofluid, Ind. Eng. Chem. Res. 53 (2014) 6677–6684, https://doi.org/10.1021/ie500705j.

[99] J. Norman, J. Wagner, Brady, Shear thickening in colloidal dispersions, Am. Inst. Phys. 48 (2009) 27–32, https://doi.org/10.1080/08856559.1936.10533734.

[100] H.A. Barnes, Shear-thickening (“Dilatancy”) in suspensions of nonaggregating solid particles dispersed in Newtonian liquids, J. Rheol. (N. Y. N. Y). 33 (1989) 329–366, https://doi.org/10.1122/1.550017.

[101] M.Z. Sharif, W.H. Azmi, A.A.M. Redhwan, R. Mamat, T.M. Yusof, Performance analysis of SiO2 /PAG nanolubricant in automotive air conditioning system, Int. J. Refrig. 75 (2017) 204–216, https://doi.org/10.1016/j.ijrefrig.2017.01.004.